Ultra-wideband optical leaky-wave slot antennas

Yan Wang, Amr S. Helmy, and George V. Eleftheriades*

The Edward S. Rogers Sr. Department of Electrical and Computer Engineering
University of Toronto, 40 St. George Street, Toronto, Ontario, M5S 2E4, Canada

**gelefth@waves.utoronto.ca*

Abstract: We propose and investigate an ultra-wideband leaky-wave antenna that operates at optical frequencies for the purpose of efficient energy coupling between localized nanoscale optical circuits and the far-field. The antenna consists of an optically narrow aluminum slot on a silicon substrate. We analyze its far-field radiation pattern in the spectral region centered around 1550nm with a 50% bandwidth ranging from 2000nm to 1200nm. This plasmonic leaky-wave slot produces a maximum far-field radiation angle at 32^o and a 3dB beamwidth of 24^o at its center wavelength. The radiation pattern is preserved within the 50% bandwidth suffering only insignificant changes in both the radiation angle and the beamwidth. This wide-band performance is quite unique when compared to other optical antenna designs. Furthermore, the antenna effective length for radiating 90% and 99.9% of the input power is only $0.5\lambda_0$ and $1.5\lambda_0$ respectively at 1550nm. The versatility and simplicity of the proposed design along with its small footprint makes it extremely attractive for integration with nano-optical components using existing technologies.

OCIS codes: (999.9999) Optical antenna; (250.5403) Plasmonics; (350.4238) Nanophotonics; (260.3910) Metal optics; (280.4788) Optical sensing.

References and links

1. W. L. Barnes, A. Dereux, and T. W. Ebbesen, "Surface plasmon subwavelength optics," Nature **424,** 824–830 (2003).
2. J. Takahara and T. Kobayashi, "From subwavelength optics to nano-optics," Opt. Photon. News **15,** 54–59 (2004).
3. E. Ozbay, "Plasmonics: merging photonics and electronics at nanoscale dimensions," Science **311,** 189–193 (2006).
4. P. Ginzburg, D. Arbel, and M. Orenstein, "Gap plasmon polariton structure for very efficient microscale-to-nanoscale interfacing," Opt. Lett. **31,** 3288–3290 (2006).
5. J. Tian, S. Yu, W. Yan, and M. Qiu, "Broadband high-efficiency surface-plasmon-plolariton coupler with silicon-metal interface," Appl. Phys. Lett. **95,** 013504 (2009).
6. P. Ginzburg and M. Orenstein, "Plasmonic transmission lines: from micro to nano scale with $\lambda/4$ impedance matching," Opt. Express **15,** 6762–6767 (2007).
7. H. Giessen and M. Lippitz, "Directing light emission from quantum dots," Science **329,** 910–911 (2010).
8. L. Novotny, "Effective wavelength scaling for optical antennas," Phys. Rev. Lett. **98,** 266802 (2007).
9. A. Alù, and N. Engheta, "Tuning the scattering response of optical nanoantennas with nanocircuit loads," Nat. Photonics **2,** 307–310 (2008).
10. T. H. Taminiau, F. D. Stefani, F. B. Segerink, and N. F. van Hulst, "Optical antennas direct single-molecule emission," Nat. Photonics **2,** 234–237 (2008).
11. E. Cubukcu, E. A. Kort, K. B. Crozier, and F. Capasso, "Plasmonic laser antenna," Appl. Phys. Lett. **89,** 093120 (2006).
12. N. Yu, E. Cubukcu, L. Diehl, D. Bour, S. Corzine, J. Zhu, G. Höfler, K. B. Crozier, and F. Capasso, "Bowtie plasmonic quantum cascade laser antenna," Opt. Express **15,** 13272–13281 (2007).

#146204 - $15.00 USD Received 19 Apr 2011; revised 23 May 2011; accepted 30 May 2011; published 10 Jun 2011

13. A. G. Curto, G. Volpe, T. H. Taminiau, M. P. Kreuzer, R. Quidant, and N. F. van Hulst, "Unidirectional emission of a quantum dot coupled to a nanoantenna," Science **329,** 930–933 (2010).
14. T. Kosako, Y. Kadoya, and H. F. Hofmann, "Directional control of light by a nano-optical Yagi-Uda antenna," Nat. Photonics **4,** 312–315 (2010).
15. X. X. Liu and A. Alù, "Subwavelength leaky-wave optical nanoantennas: directive radiation from linear arrays of plasmonic nanoparticles," Phys. Rev. B **82,** 144305 (2010).
16. P. Bharadwaj, B. Deutsch, and L. Novotny, "Optical antennas," Adv. Opt. Photon. **1,** 438–483 (2009).
17. A. Neto and S. Maci, "Green's function for an infinite slot printed between two homogeneous dielectrics - part I: magnetic currents," IEEE Trans. Antennas Propag. **51,** 1572–1581 (2003).
18. A. Neto and S. Maci, "Green's function for an infinite slot printed between two homogeneous dielectrics - part II: uniform asymptotic solution," IEEE Trans. Antennas Propag. **52,** 666–676 (2004).
19. G. V. Eleftheriades and G. M. Rebeiz, "Self and mutual admittance of slot antennas on a dielectric half-space," Int. J. Infrared Millim. Waves **14,** 1925–1946 (1993).
20. C. A. Balanis, *Antenna Theory: Analysis and Design*, 3rd ed. (Wiley, 2005), Chap. 10.
21. A. D. Rakić, A. B. Djurišić, J. M. Elazar, and M. L. Majewski, "Optical properties of metallic films for vertical-cavity optoelectronic devices," Appl. Opt. **37,** 5271–5283 (1998).
22. J. J. Burke, G. I. Stegeman, and T. Tamir, "Surface-polariton-like waves guided by thin, lossy metal films," Phys. Rev. B **33,** 55186–5201 (1986).
23. Y. Wang, R. Islam, and G. V. Eleftheriades, "An ultra-short contra-directional coupler utilizing surface plasmon-polaritons at optical frequencies," Opt. Express **14,** 7279–7290 (2006).
24. G. Veronis and S. Fan, "Guided subwavelength plasmonic mode supported by a slot in a thin metal film," Opt. Lett. **30,** 3359–3361 (2005).

1. Introduction

The emerging field of nano-photonics has been gaining significant attention in recent years. As such, the interest in plasmonics, and in particular plasmonic optical antennas has been growing rapidly. Plasmonic optical antennas bridge two domains, namely, surface plasmon polaritons (SPPs) and radio frequency (RF) antennas. Surface plasmon polaritons are electromagnetic waves that take place at the metal-dielectric interface at optical frequencies. The tight mode confinement associated with SPPs, which is on the order of a few tens of nanometers has attracted substantial attention recently [1–3]. RF antennas, on the other hand, are well known for efficiently converting the energy localized in devices, guided waves or circuits into free-space radiation. This conversion is important because it not only enables signal transmission/reception wirelessly, but also bridges two very different length scales; namely extreme sub-wavelength circuits and free-space. At optical frequencies, the need for interconnecting sub-wavelength circuits and free-space is essential in many areas. One example is optical interconnects, where the energy coupling between off-chip light sources and on-chip nanoscale guided waves has often been challenging and inefficient due to the size mismatch between both domains. Common matching schemes, such as coupling through various tapered dielectric waveguides, often lead to a large footprint for the overall circuit size and also suffer from tremendous losses [4,5]. Some resonant structures have been introduced in order to reduce the coupling length but are essentially narrowband [6]. Another area that demands the effective coupling of free-space with nano-optical elements is the emission enhancement of nano-scale emitters. Examples include stimulated emission from single quantum dots, luminescence from single biological molecules as well as scattering from metal nanoparticles tagged with biological specimens, where surface enhanced Raman (SERS) effects take place. In such systems, the spectrum of the excitation/emission can range from a few hundred nanometers to a few microns. On the other hand, the emitter size is on the order of only a few tens of nanometers. Such a scale mismatch is challenging for the energy conversion because small circuit elements lead to inefficient coupling with free-space due to their impedance mismatch [7]. For example, an elementary dipole and a quantum dot are both extremely poor radiators at RF and optical frequencies respectively. This problem can be alleviated by coupling the nanoscale localized energy through an optical antenna because it provides better matching to free-space. Additionally, the radiation direc-

#146204 - $15.00 USD Received 19 Apr 2011; revised 23 May 2011; accepted 30 May 2011; published 10 Jun 2011

tion and polarization are primarily determined by the antenna characteristics, which render the coupling more directive instead of omni-directional. Therefore, antennas with very high directivity, such as the family of traveling-wave antennas, are particularly well suited to address the aforementioned applications.

Despite their potential, optical antennas have experienced slow progress compared to their RF counterparts. Ever since the theoretical concept of plasmonic antennas was introduced [8,9], several basic designs such as the plasmonic monopole, the dipole, and the bowtie antennas have been investigated for their near-field interaction with localized energy sources [10–12]. Recent interest in the far-field radiation characteristics have spawned research utilizing antennas with high directivity, such as the optical Yagi-Uda antenna and the leaky-wave nano-particle chain, because they can direct emission and reception within a small solid angle [13–15]. However, one limitation of these existing designs is that they rely on resonant structures, which are inherently narrowband. The ability of interacting with light over a wide spectrum is desirable in many domains, such as coupling a broad spectrum of light for optical interconnects, providing a large spectral response in spectroscopy, and harvesting a wide range of light in photoconductive devices [16]. To overcome this bandwidth limitation requires the elimination of the resonance effects, which is one of the main contributions of this work.

The design we propose in this work is a leaky-wave antenna, which belongs to the general class of traveling-wave antennas known for their high directivity. Our structure utilizes the leaky-mode of a plasmonic slot waveguide (PSW) as illustrated in Fig. 1. Unlike existing designs, sharp directivity can be experienced over a wide frequency range. It is also important to point out that besides ultra wideband radiation, this structure is much more feasible to fabricate, due to its lower sensitivity to the structure dimensions. Fabrication tolerances on this size scale can pose serious impediments for achieving a desired functionality through the use of highly resonant structures.

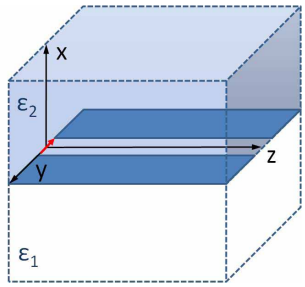

Fig. 1. The geometry of the proposed plasmonic leaky-wave antenna. The structure consists of a metallic (aluminum) slot placed between two dielectric half-spaces. In our design, the upper medium is silicon and the lower one is air. The slot is 46nm thick and 46nm wide, which corresponds to about $0.03\lambda_0$ at the center operating wavelength of 1550nm. The leaky mode along the slot is excited by an electric dipole (the red arrow) at z = 0, and it radiates energy into the silicon upper space.

2. Background and theory

2.1. Leaky-wave slot antenna

The theory of this work is inspired by the analysis for an infinite perfect-electric-conductor (PEC) slot placed between two homogeneous dielectrics, similar to the one shown in Fig. 1 [17, 18]. The PEC is assumed to have an infinitesimal thickness and the slot width is very small compared to the wavelength (less than $1/10\lambda_0$). Using the analytical closed-form solution of the

#146204 - $15.00 USD Received 19 Apr 2011; revised 23 May 2011; accepted 30 May 2011; published 10 Jun 2011

Green's function [19], the asymptotic solutions are calculated to reveal the leaky-wave radiation pattern, which is of a half-conical shape in the dense medium as shown in Fig. 2(a). The energy in the air is negligible compared to silicon. For traveling-wave antennas, the radiation angle θ and the beamwidth shown in Fig. 2(b) are determined by the complex propagation constant of the traveling wave, which is the leaky slot mode in this case. More specifically, the radiation angle depends on the phase constant β and the beamwidth reflects the leakage constant α. Intuitively, a wider slot leads to a faster leakage, which results in a wider beam.

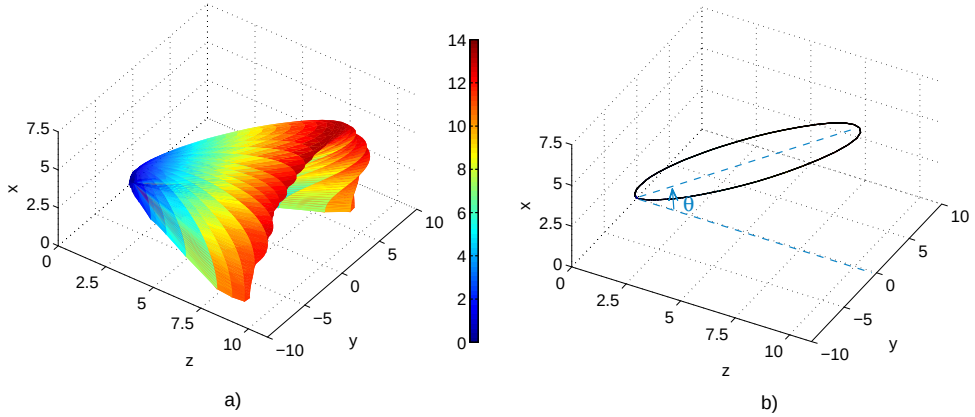

Fig. 2. The directivity of the PEC slot antenna placed between silicon and air. The schematic of the structure is illustrated in Fig. 1. The simulation is conducted in ADS Momentum by *Agilent Technologies* based on the method of moments (MoM). The slot antenna operates at 1550nm. (a) 3D directivity pattern; (b) 2D directivity pattern in the H-plane.

From the phase and leakage constants, the far-field magnetic field can be derived in the H-plane according to Eq. (1) [20].

$$H_\theta = j\frac{k_2 I_{m0} l}{\eta_2}\frac{e^{-jk_2 r}}{4\pi r} sin\theta \left(e^{j\frac{k_2 l}{2}(cos\theta - K)}\right) \frac{sin\left(\frac{k_2 l}{2}(cos\theta - K)\right)}{\frac{k_2 l}{2}(cos\theta - K)} \tag{1}$$

where I_{m0} is the equivalent (fictitious) magnetic current in the slot, k_2 and η_2 refer to the propagation constant and the wave impedance of silicon respectively. Moreover, $K = (\beta + j\alpha)/k_2$ is the normalized propagation constant of the leaky mode. Quantities l and r represent the length of the slot and the observation distance. The H-field in medium 1 (air) is derived using the same formula and shown to be negligible compared to that in medium 2 (silicon). Finally, the radiation pattern for the power density in the silicon regime is calculated as shown in Eq. (2).

$$P_\theta = \frac{1}{2}\eta_2 |H_\theta|^2 \tag{2}$$

The interesting feature of this leaky-wave antenna is that the radiation angle is almost frequency invariant, because the phase constant β is primarily determined by the relative electric permittivity of the two dielectric media as described in Eq. (3).

$$\cos(\theta) = \frac{\beta}{k_2} \approx \sqrt{\frac{\varepsilon_1 + \varepsilon_2}{2\varepsilon_2}} \tag{3}$$

This approximation holds true when the slot is very narrow compared to the wavelength. In fact, the wavelength variation affects the leakage constant α more because the slot width changes in

#146204 - $15.00 USD Received 19 Apr 2011; revised 23 May 2011; accepted 30 May 2011; published 10 Jun 2011

terms of its optical length. In order to demonstrate the impact of the wavelength variation quantitatively, a sensitivity analysis is conducted to illustrate the dispersion properties of the leaky mode. More specifically, Fig. 3 illustrates the effect of varying the slot width, from which the wavelength-dependence can be deduced. In Fig. 3(a), the two horizontal black lines correspond to the light lines in air (lower) and silicon (upper). This confirms that the phase constant of the leaky mode is slow compared to the propagation in air, but fast compared to the one in silicon, which explains the energy leakage into the denser silicon medium. Figure 3(b) illustrates that the leakage increases when the wavelength decreases as expected.

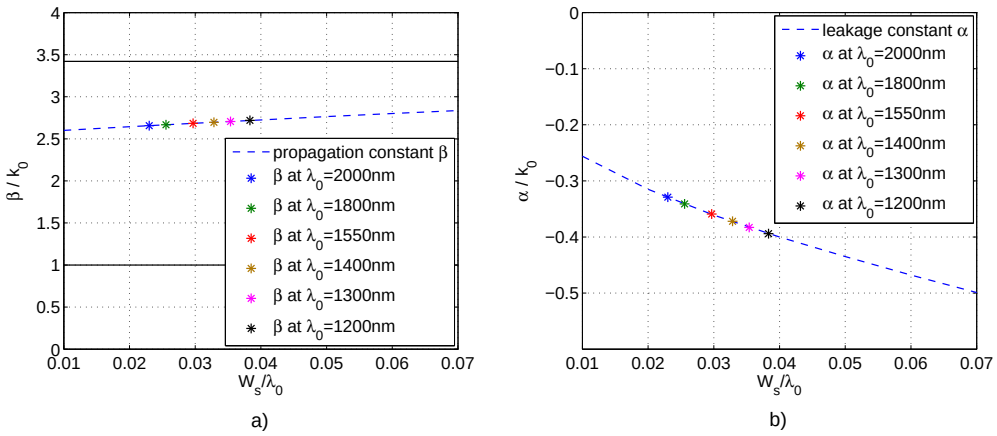

Fig. 3. The normalized complex propagation constant (the effective mode index) of the leaky mode for an infinite PEC slot placed between silicon and air. The slot width is fixed at 46nm, which corresponds to $0.03\lambda_0$ at 1550nm. The spectrum ranges from 2000nm to 1200nm. The data is obtained from the eigenmode analysis in Comsol Multiphysics by *Comsol Inc.* (a) Phase constant β; (b) Leakage constant α.

Furthermore, the impact of the wavelength dispersion on the radiation pattern is illustrated in Fig. 4, which confirms that the beamwidth increases only slightly with the optical length of the slot width, but the radiation angle remains relatively unchanged. From these analyses, we can conclude that this structure is a good platform, from which a wideband plasmonic leaky-wave antenna can be implemented.

2.2. Plasmonic slot waveguides (PSWs)

At optical frequencies, the metal is described with a Drude or Debye model instead of being approximated with PEC. The dispersion of the electric permittivity of metals, such as silver, gold and aluminum, is illustrated in Fig. 5 [21]. The negative real component of the electric permittivity shown in Fig. 5(a) indicates that surface waves, SPPs, can be supported at the metal and dielectric interfaces. The imaginary component in Fig. 5(b) represents the loss of the metal. Additionally, coupled SPP modes are formed when two or more single-interface SPPs are brought within proximity of each other.

Before discussing the properties of an asymmetric plasmonic leaky slot (PLS) placed between air and silicon, it is instructive to first discuss the symmetric plasmonic slot waveguide (PSW) embedded only in air. Compared to the TEM mode in a thin PEC slot waveguide, the TE-mode guided by the PSW is a slower mode, whose effective mode index is enhanced (propagation slowed down) due to the negative electric permittivity of the metal. As illustrated in Fig. 5(a), metals such as aluminum, gold and silver all have a negative electric permittivity

#146204 - $15.00 USD Received 19 Apr 2011; revised 23 May 2011; accepted 30 May 2011; published 10 Jun 2011

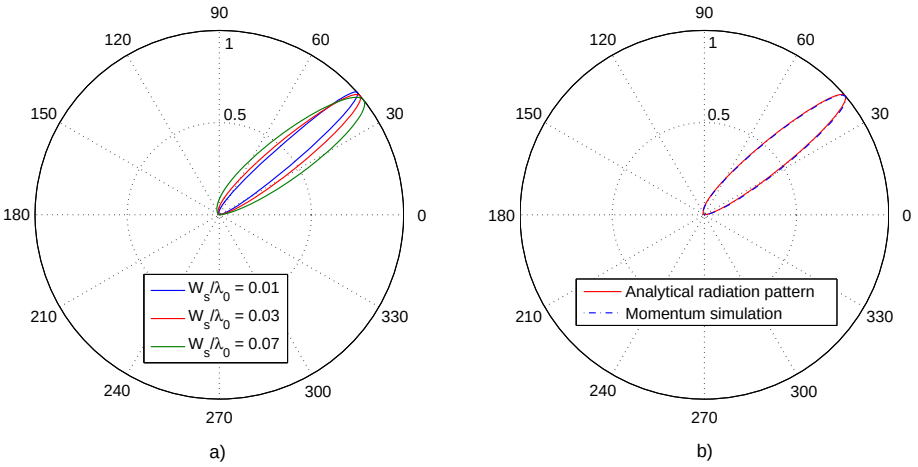

Fig. 4. The normalized directivity pattern in the H-plane for an infinite PEC slot placed between air and silicon. The results are based on the theoretical calculation using Eq. (2) and the complex propagation constant in Fig. 3. (a) Normalized directivity for the slot width ranging from $0.01\lambda_0$ to $0.07\lambda_0$; (b) Comparison between the theoretical calculation and the MoM simulation at 1550nm.

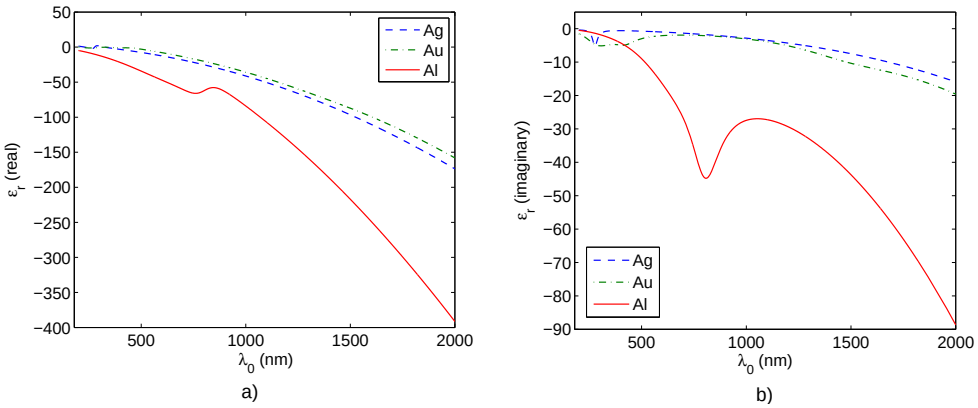

Fig. 5. The dispersion diagrams of the relative electric permittivity of gold, silver and aluminum at optical frequencies. (a) Real component; (b) Imaginary component.

#146204 - $15.00 USD Received 19 Apr 2011; revised 23 May 2011; accepted 30 May 2011; published 10 Jun 2011

at optical frequencies. Since the negative ε_r of aluminum is larger in magnitude compared to gold and silver, it behaves closer to a PEC in the optical regime. In other words, the mode guided by an aluminum slot will be slower than that of a PEC slot, but faster than those of gold or silver. This can be explained by the fact that the surface mode is known to slow down significantly close to the spectral region near the transverse resonance condition, where $|\varepsilon_{metal}| = \varepsilon_{dielectric}$ [22, 23]. A negative electric permittivity with a larger magnitude in the optical regime implies that the transverse resonance condition takes place at a much shorter wavelength for aluminum compared to gold and silver. Therefore, the fundamental guided mode (a forward even mode) in an aluminum slot propagates closer to the light line in the spectral regime of interest.

The enhancement of the effective mode index could pose challenges in an asymmetric structure, such as our leaky-wave antenna, if the slot mode is slower than the propagation constant in the dense medium. In such cases the energy will not leak out of the slot mode and hence would prohibit radiation. Some versions of PSW on a dielectric substrate that operate at 1550nm with a similar geometry as our PLS have been reported previously [24]. The reason that such designs support the bound/guided fundamental mode instead of the leaky mode is that silver has been utilized. To the best of our knowledge, aluminum presents the optimum option for our plasmonic material at optical frequencies in order to facilitate a fast slot mode similar to the one in the PEC leaky-wave antenna at microwave frequencies.

3. Characteristics of plasmonic leaky slot antennas

When the PSW is placed on a dense substrate/cladding, the guided slot mode becomes a fast wave with respect to the dense medium. Therefore, we can obtain a similar leaky-wave radiation as the PEC slot as illustrated in Fig. 2. In order to analyze the wavelength dependence of the radiation characteristics, we also extract the dispersion diagrams for the normalized complex propagation constant of the slot mode in Fig. 6. From this analysis, we conclude that there are three important differences between the PEC leaky-wave antenna and the PLS antenna. First, the phase constant β of the PLS antenna cannot be accurately predicted by the approximation in Eq. (3) because it does not account for the wavelength dispersion of the metal. Fig. 6(a) shows that besides having a larger phase constant, the PLS antenna does not possess a linear relationship between β and λ_0, such as the one seen in Fig. 3(a) for a PEC leaky-wave slot. This implication will be discussed later in this section. Second, the effective mode index increases beyond the refractive index of silicon (the solid horizontal black line in Fig. 6(a)) below 1100nm, which indicates the absence of radiation for the fundamental mode because it becomes a bounded mode. This is not abserved for PEC leaky slot antennas. Finally, the attenuation constant α is affected by the radiation rate as well as the dissipation in the metal. This additional loss mechanism decreases the efficiency of the antenna since not all of the input energy is radiated. The effect of dissipation is more pronounced at shorter wavelengths because the mode penetrates deeper into the plasmonic metal. The efficiency of our PLS antenna will be discussed later in the section.

These differences are reflected in their radiation patterns shown in Fig. 7. In Fig. 7(a), the larger phase constant β of our PLS antenna leads to a smaller radiation angle compared to its PEC counterpart at the same wavelength. Additionally, as illustrated in Fig. 7(b), the nonlinearity between β and λ_0 results in the observed slight beam-squinting (change in the radiation angle) when the wavelength is varied. The beamwidth also increases visibly at shorter wavelengths due to the metallic loss as illustrated in Fig. 7(c).

Although theoretically it takes an infinite leaky-wave slot to radiate all the input energy, the exponential decay of the slot mode along the z-direction indicates that a PLS antenna with a short finite length could be very effective to approximate an infinite slot. Based on the attenu-

#146204 - $15.00 USD Received 19 Apr 2011; revised 23 May 2011; accepted 30 May 2011; published 10 Jun 2011

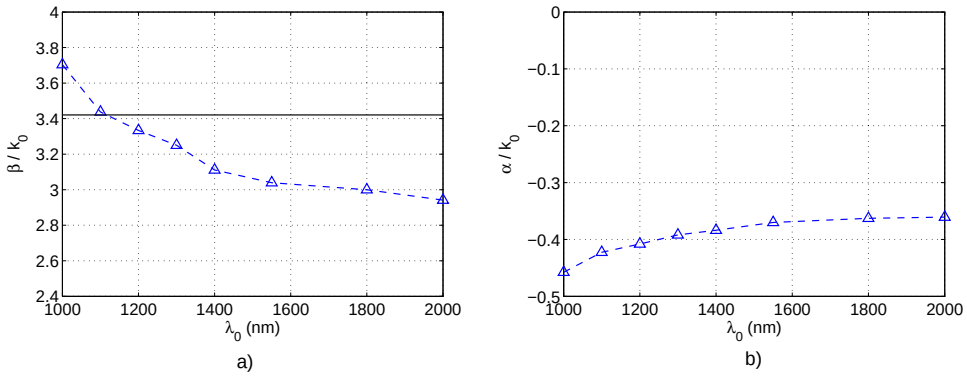

Fig. 6. The normalized complex propagation constant (the effective mode index) of the slot mode for an infinite PLS placed between air and silicon. The aluminum slot is 46nm thick and 46nm wide. The spectrum of our interest centers at 1550nm and ranges from 2000nm to 1200nm. The data is obtained through the 3D full-wave simulations in Comsol Multiphysics by *Comsol Inc.* (a) Phase constant β; (b) Attenuation constant α.

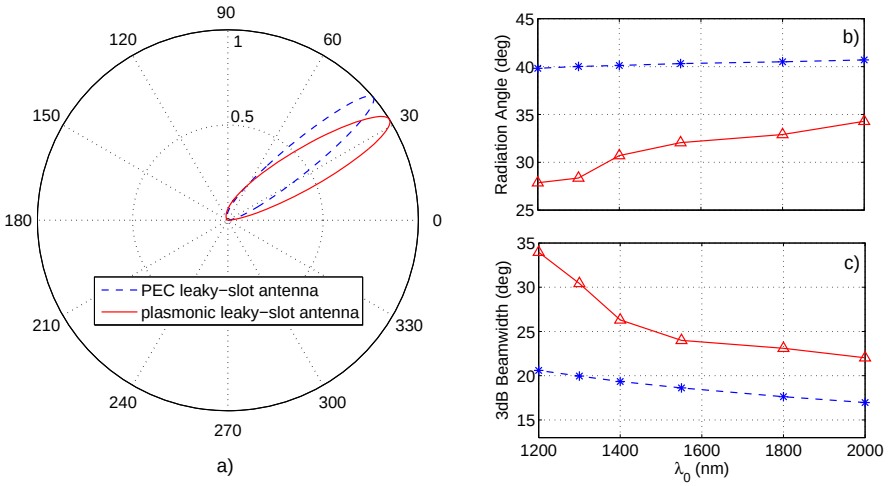

Fig. 7. The comparison of the radiation pattern for an infinite PEC leaky slot and a PLS antenna of the same dimension. (a) The radiation pattern at the center wavelength of 1550nm; (b) The radiation angle variation (squinting) with wavelength; (c) The 3dB beamwidth fluctuation with wavelength.

#146204 - $15.00 USD Received 19 Apr 2011; revised 23 May 2011; accepted 30 May 2011; published 10 Jun 2011

ation constant α in Fig. 6(b), the required length to radiate (including dissipation) 90% of the input power is $0.5\lambda_0$ (or $1.69\lambda_{silicon}$). An infinite slot with 99.9% radiation (including dissipation) can be approximated with a slot length of $1.5\lambda_0$. This short slot length is important for reducing the footprint of the radiating element with appropriate design. In terms of antenna efficiency, which is defined as $P_{radiated}/P_{input}$, the performance of the PLS antenna is hindered by the metallic loss as discussed before. More specifically, for a slot that is long enough to leak 90% of the input power, only 73.5% is converted into radiation. Thus the plasmonic antenna efficiency is estimated to be 73.5% for the slot with a length $0.5\lambda_0$ at the nominal wavelength of 1550nm as illustrated in Fig. 8.

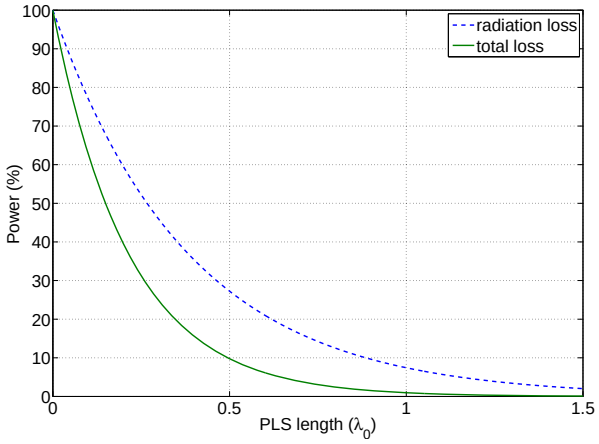

Fig. 8. The power remained in the PLS antenna with respect to the input at 1550nm. The dashed line represents the situation where only the radiation loss is accounted for. The solid line represents the one where both the radiation and the metallic dissipation are present.

The wavelength range between 1200nm to 2000nm represents a spectrum with 50% bandwidth centered at 1550nm. This bandwidth is well beyond the wideband definition for antennas. It is instructive to note that we choose to analyze the spectrum below 2000nm due to the availability of data for the electric permittivity of aluminum. Although our analysis is limited by an upper bound wavelength, this leaky-wave antenna could operate well beyond that limit at longer wavelengths. In fact, the PLS antenna will follow closer to the behavior of the PEC leaky-wave antenna at longer wavelengths due to the dramatically increased negative electric permittivity. The slot width is optically smaller at longer wavelengths, which leads to an even higher directivity. This trend can be seen from Fig. 7(b) and 7(c), where both the radiation angle and the beamwidth of the PLS antenna approach its PEC counterpart as the wavelength increases. This is a significant bandwidth enhancement compared to the existing traveling-wave antennas at optical frequencies with similar beamwidths. For example, the leaky plasmonic-sphere chain only produces a directive beam within the range of 680nm to 740nm, and the bandwidth for the optical Yagi-Uda antenna is only 150nm centered at around 800nm [13, 15].

Finally, we like to stress the benefit of our proposed structure from the point of view of its practical implementation. The wideband behavior makes the PLS antenna less prone to fabrication imperfection tolerances because optical length scale variations do not affect its performance very much. One example of sensitivity analysis is illustrated in Fig. 9, where the thickness of the aluminum is varied by 10% with respect to its nominal value of 46nm. We can see that this 10% variation does not change the radiation pattern much in terms of both the radiation angle and the beamwidth. This is especially attractive to circumvent the fabrication

#146204 - $15.00 USD Received 19 Apr 2011; revised 23 May 2011; accepted 30 May 2011; published 10 Jun 2011

tolerance of nano-scale features.

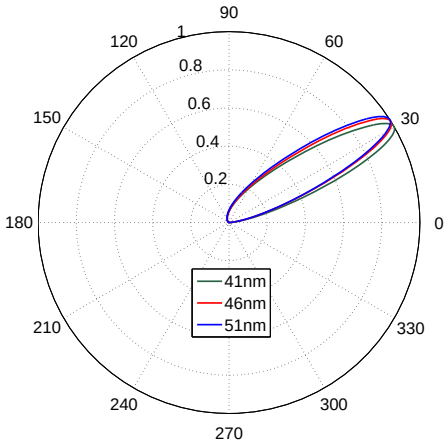

Fig. 9. The effect of 10% variation in the aluminum film thickness on the radiation pattern at 1550nm.

In summary, the PLS antenna that operates at 1550nm produces a radiation angle of 32^o and a 3dB beamwidth of 23.8^o. The range of deviation in the radiation angle and the 3dB beamwidth are $[-4.4^o, 1.8^o]$ and $[+9.8^o, -3.3^o]$ when the wavelength varies from 1200nm to 2000nm respectively. At 1550nm, the estimated antenna efficiency is 73.5% for a slot length of $0.5\lambda_0$.

4. Conclusion

In conclusion, we present a leaky-wave slot antenna at optical frequencies that achieves a wide-band operation, which is centered at 1550nm with a 50% bandwidth that ranges from 2000nm to 1200nm. Compared to existing optical antennas that rely on resonant structures, our design consists of a simple sub-wavelength (in width and thickness) aluminum slot placed on silicon. The absence of any resonant elements gives rise to a wideband behavior, which is insensitive to small fabrication tolerances. It is also observed that due to the dispersion of the electric permittivity of aluminum at optical frequencies, the leaky-mode of our slot antenna has a lower bound limit at 1100nm, below which the leaky mode becomes a bounded mode. This is not observed for PEC leaky slot antennas. The radiation pattern of the PLS antenna approaches the one of its PEC counterpart with increasing wavelength. Although our analysis is performed for the spectrum from 2000nm to 1200nm, the PLS antenna is expected to operate at longer wavelengths with an even more directive far-field radiation pattern. Furthermore, this design can be extended by placing an array of slots side-by-side (along the y-axis in Fig. 1) to increase the directivity in the E-plane (the xy-plane). In this way, the half-conical beam shape of Fig. 2 can be transformed into a pencil beam if so desired. We foresee these proposed wideband leaky-wave antennas or arrays to be very useful for the efficient conversion of localized energy in subwavelength dimensions to free space.

#146204 - $15.00 USD Received 19 Apr 2011; revised 23 May 2011; accepted 30 May 2011; published 10 Jun 2011